THE JOURNAL OF PHYSICAL CHEMISTRY Letters

pubs.acs.org/JPCL Letter

Development of Novel Mixed Halide/Superhalide Tin-Based Perovskites for Mesoscopic Carbon-Based Solar Cells

Mohammad Rameez, Saeed Shahbazi, Putikam Raghunath, Ming Chang Lin, Chen Hsiung Hung,* and Eric Wei-Guang Diau*

Cite This: *J. Phys. Chem. Lett.* 2020, 11, 2443−2448 Read Online

ACCESS | Metrics & More | Article Recommendations | Supporting Information

ABSTRACT: Tin perovskites suffer from poor stability and a self-doping effect. To solve this problem, we synthesized novel tin perovskites based on superhalide with varied ratios of tetrafluoroborate to iodide and implemented them into solar cells based on a mesoscopic carbon-electrode architecture because film formation was an issue in applying this material for a planar heterojunction device structure. We undertook quantum-chemical calculations based on plane-wave density functional theory (DFT) methods and explored the structural and electronic properties of tin perovskites $FASnI_{3-x}(BF_4)_x$ in the series x = 0, 1, 2, and 3. We found that only the x = 2 case, $FASnI(BF_4)_2$, was successfully produced, beyond the standard $FASnI_3$. The electrochemical impedance and X-ray photoelectron spectra indicate that the addition of tin tetrafluoroborate instead of SnI_2 suppressed trap-assisted recombination by decreasing the Sn^{4+} content. The power conversion efficiency of the $FASnI(BF_4)_2$ device with FAI and $Sn(BF_4)_2$ in an equimolar ratio improved 72% relative to that of a standard $FASnI_3$ solar cell, with satisfactory photostability under ambient air conditions.

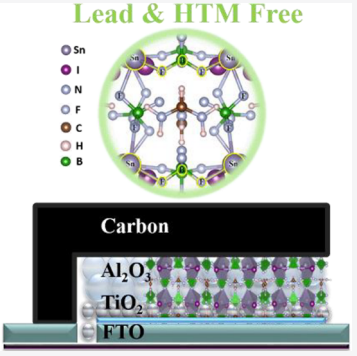

Photovoltaics based on perovskites have attracted considerable attention with perovskite solar cells (PSCs) achieving a power conversion efficiency (PCE) of >25%.[1] Band gap tuning and solution deposition are their key features for the use of these materials in various fields.[2] Nevertheless, traditional PSCs suffer from two major problems: stability and toxicity of lead.[3] Many schemes have been proposed for the replacement of lead.[3−6] Among them, a tin-based PSC is the most promising with a PCE of 10% being reported.[7] They have band gaps smaller than those of their lead analogues, showed promising properties as light absorbers, and can be a suitable replacement for the highly toxic lead-based perovskites, but these tin-based perovskites suffer from poor stability.[8] To overcome these stability issues, various approaches such as the use of reducing reagents and organic and inorganic additives or co-additives have been proposed to suppress intrinsic Sn^{2+}/Sn^{4+} oxidation. Various cations have also been used to improve the stability, e.g., cesium (Cs^+), formamidinium (FA^+), guanidinium (GA^+), etc.[9−14]

Apart from the cations, anions such as various pseudohalides (SCN^-) and superhalides (BF_4^- and PF_6^-) are known to increase the stability and to passivate the trap states for lead-based PSCs.[15−21] Tin superhalides are poorly conducting in the polaronic hopping limit; they might hence be effective in decreasing the carrier density in tin-based PSCs.[19] A mixed-halide (I^- and BF_4^-) perovskite possesses a low-frequency conductivity that is 10 times that of an I^--based perovskite without an appreciable change in the absorption onset.[15] The incorporation of a fluoroborate anion into the perovskite structure suppresses recombination, resulting in superior device performance.[20,21] Xiang et al.[22] theoretically investigated the incorporation of BH_4 and AlH_4 superhalides that enhanced the oxidation resistance of Sn^{2+} in $MASnI_3$ perovskites. To the best of our knowledge, no theoretical or experimental data concerning tin-based tetrafluoroborate perovskites have been reported.

Superhalide anion BF_4^- is less nucleophilic and basic than nitrates and halides; as its structure is symmetric, it can occupy the position of I^- in a perovskite crystal structure. Moreover, BF_4^- is composed of highly electronegative fluorine atoms; the corresponding perovskites might be more stable toward hydrolysis than conventional tin perovskites (e.g., $FASnI_3$). Herein, we report the development of a novel lead-free BF_4^--based photovoltaic material as a light harvester employing superhalide anion BF_4^- with a suitable band gap (E_g) of ∼1.36 eV. Furthermore, we varied the BF_4^-:I^- ratio to assess the feasibility of formation of perovskites and studied their crystal structures via quantum-chemical calculations to compare them with the X-ray diffraction (XRD) data. X-ray photoelectron spectroscopy (XPS) results showed an increased concentration of element F, hence proving the presence of BF_4^- in the perovskite crystal.

Received: February 13, 2020
Accepted: March 12, 2020
Published: March 12, 2020

https://dx.doi.org/10.1021/acs.jpclett.0c00479
J. Phys. Chem. Lett. 2020, 11, 2443−2448

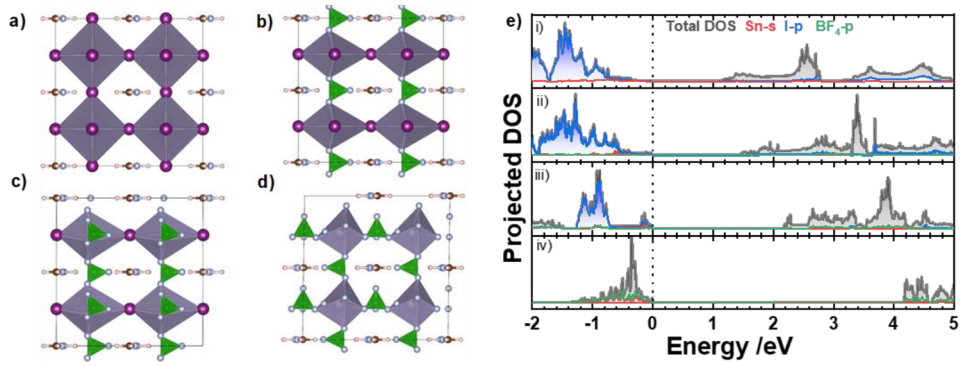

Figure 1. Simulated DFT crystal structures of perovskites $FASnI_{3-x}(BF_4)_x$ with x values of (a) 0, (b) 1, (c) 2, and (d) 3. (e) Simulated projected density of states (PDOS) of perovskites $FASnI_{3-x}(BF_4)_x$ with x values of (i) 0, (ii) 1, (iii) 2, and (iv) 3.

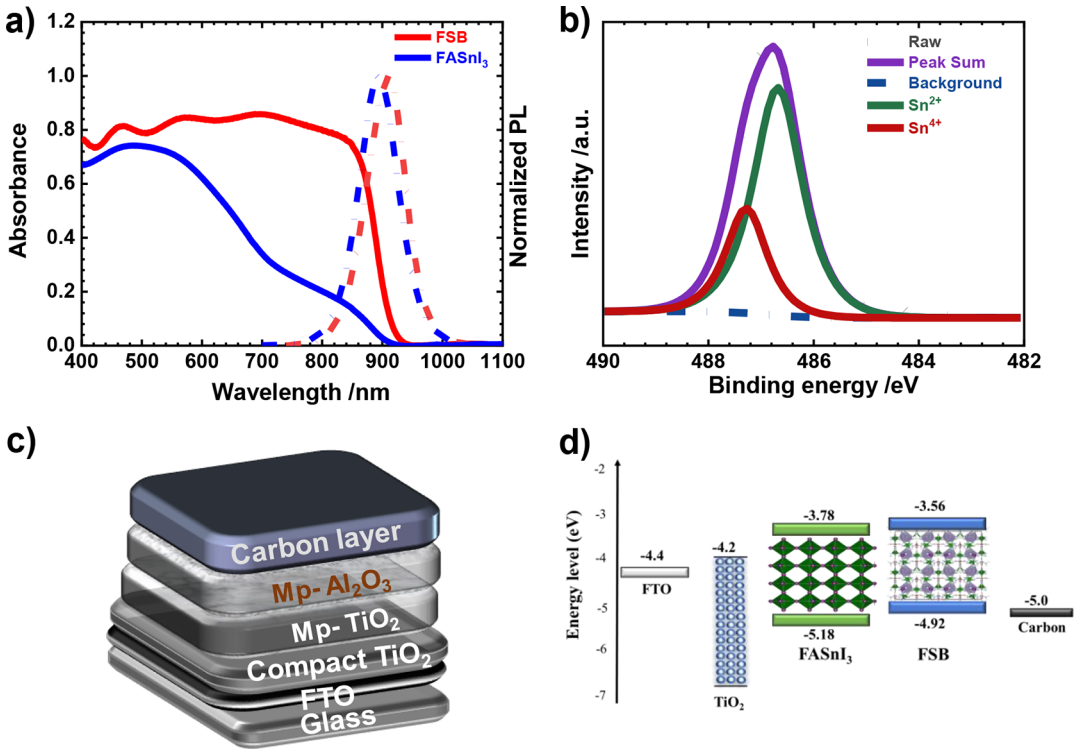

Figure 2. (a) Absorption (solid curves) and normalized PL (dashed curves) spectra of FSB and $FASnI_3$ films deposited on glass substrates. (b) XPS of tin species for FSB. (c) Mesoporous carbon-based device structure. (d) Potential energy levels [energies (electronvolts) with respect to vacuum] of FSB and $FASnI_3$ compared with those of TiO_2 and carbon.

To evaluate the possibility of the formation of 3D perovskites, we undertook quantum-chemical calculations based on plane-wave density functional theory (DFT) with the Vienna *ab initio* simulation package (VASP). Beginning with experimental phase *Amm2* in perovskite $FASnI_3$,[23] the simulated crystal structures of perovskites $FASnI_{3-x}(BF_4)_x$ (x = 0, 1, 2, and 3) are shown in panels a–d of Figure 1, respectively. The symmetry of the optimized $FASnI_{3-x}(BF_4)_x$ structure shows a 6-fold-coordinated octahedron with organic FA cations occupying the $[SnX_6]^{4-}$ (X = I^- or BF_4^-) octahedral holes with an increase in the unit-cell volume with an increase in BF_4^- content. The fully optimized lattice parameters of $FASnI_{3-x}(BF_4)_x$ with representative space groups are listed in Table S1. We also calculated the tolerance factor (α) and octahedral factor (μ), values of which are listed in Table S2.[24] For $FASnI_{3-x}(BF_4)_x$, the tolerance factor decreases slightly with an increase in x; the octahedral factors exhibit a similar trend. These results indicate that increasing the number of BF_4^- ions in perovskites leads to an enhancement of the B-site metal–octahedron contact. Calculated lengths of the Sn–X bond decrease (Table S3) with an increase in the number of BF_4^- anions, which is attributed mainly to the varied electronegativity values. To understand further the electronic structures of mixed iodide–tetrafluoroborate perovskites, we calculated the total projected densities of states (PDOS), shown in Figure 1e. Organic cations typically maintain only overall charge neutrality and structural stability but play no significant role in the optical and electronic properties of the perovskite.[25] We hence present the PDOS of only Sn with halide and superhalide. In the $FASnI_{3-x}(BF_4)_x$ system, Sn s and halide or superhalide p orbitals form the valence band maximum (VBM). The conduction band minimum (CBM) consists mostly of halide or superhalide p orbitals. The calculated band gaps for

https://dx.doi.org/10.1021/acs.jpclett.0c00479
J. Phys. Chem. Lett. 2020, 11, 2443–2448

$FASnI_{3-x}(BF_4)_x$ are 1.1 eV ($x = 0$), 1.44 eV ($x = 1$), 2.01 eV ($x = 2$), and 4.1 eV ($x = 3$); the band gaps of $FASnI_{3-x}(BF_4)_x$ hence become tunable by controlling the BF_4^- content. The band gap for $x = 2$, henceforth called FSB, was further calculated to be 1.78 eV (Figure S1) using a Heyd−Scuseria−Ernzerhof (HSE) exchange-correlation function. Our calculated band gaps agree satisfactorily with previous theoretical work on $FASnI_3$.[26,27] Both the CBM and the VBM are isotropic and dispersive, indicating small effective masses of carriers. One can see from the PDOS (Figure S2) that the energy levels of the Sn 5s orbitals were shifted to more positive values. The Sn vacancy defects have formation energies consequently less for $FASnI_3$ than for FSB under similar growth conditions; we accordingly infer a device performance for the former that is poorer than that for the latter.[26] The calculated formation enthalpies are summarized in Table S4; the calculated enthalpy of formation is the lowest for FSB.

Given the suitable band gaps and appropriate tolerance factors, we turn to our experimental investigation of $FASnI_{3-x}(BF_4)_x$ films. These films were prepared with equimolar stoichiometric proportions of formamidinium and tin salts (FAX and SnX_2, where X = I^- or BF_4^-); the experimental details are presented in the Supporting Information. The pictures of the solutions with the corresponding films shown in Figure S3 indicate that no stable perovskite film was produced in the $x = 1$ and 3 cases, confirmed with the XRD patterns (Figure S4). However, for the $x = 0$ and 2 cases, the characteristic XRD features of tin perovskites are clearly shown. When $FABF_4$ served as a precursor to obtain perovskites with $x = 1$ and 3, the characteristic XRD signal at 14.0° was missing. For perovskite deposition via a wet process, incorporation of the formamidinium salt in the lattice and its further intercalation in SnX_6^- layers should have a fairly small activation energy.[28,29] We expect, however, that greater activation energies are required in the case of $FABF_4$ because of their different symmetries that could result in incomplete perovskite formation.[28] Calculation of the enthalpy of formation for $FASnI_3$ from $FABF_4$ and FAI precursors indicated that using the $FABF_4$ precursor is thermodynamically less favorable than using the FAI precursor to form the BF_4-based tin perovskites (Table S5). As, in the XRD patterns of the precursors shown in Figure S4b, no trace of precursor was found in the final perovskite (FSB) with FAI and $Sn(BF_4)_2$ in equimolar stoichiometric proportions, only a film of FSB was further characterized; the corresponding solar-cell devices were fabricated and are discussed.

The XRD patterns obtained from the DFT-calculated FSB structure are shown in Figure S5 for comparison with the experimental ones. The simulated XRD patterns match satisfactorily the experimental data after fitting. The FSB film showed characteristic XRD signals at 14.0°, 24.3°, 28.2°, and 32.0° corresponding to crystallographic planes (002), (222), (004), and (024) of FSB, respectively (Figure S5).

To visualize the optical properties, we recorded ultraviolet−visible (UV−vis) absorption and photoluminescence (PL) spectra; the corresponding results for $FASnI_3$ and FSB are shown in Figure 2a. The FSB film exhibits strong absorption within the entire visible to near-infrared spectral region. As discussed by Kato et al.,[30] the enlarged N−I distance increases optical absorption transition strengths in the vicinity above the band gap attributed to the anticoupling effect. Similarly, we observed an increase in the N−I distance from 3.81 Å in $FASnI_3$ to 3.89 Å in FSB (Figure S6), reflecting the higher above-gap optical absorption in FSB than in $FASnI_3$. A red shift in the absorption spectral band edge occurs from 890 nm ($E_g = 1.39 \pm 0.01$ eV) for $FASnI_3$ to 910 nm ($E_g = 1.36 \pm 0.01$ eV) for FSB. The decreased band gap with BF_4^- substitution is attributed to the ionic radius of BF_4^- (232 pm), which is larger than that of I^- (215 pm). A lattice relaxation might be more significant with a larger anion for the former than for the latter. As a result, this relaxation might suppress point defects, resulting in a red shift in the PL spectrum of FSB shown in Figure 2a.[18] In contrast, the calculated band gaps showed an opposite trend compared to that of the experimental results, indicating the large uncertainties involved in the estimation of band gaps for tin perovskites.[26]

To determine the position of the maximum of the valence band (VBM) and the elemental composition, we performed ultraviolet photoelectron spectroscopy (UPS) and X-ray photoelectron spectroscopy (XPS) in survey scans, shown in Figures S7 and S8, respectively. The UPS data of both perovskites indicate an upward shift in the VBM of FSB relative to that of $FASnI_3$, which is consistent with the theoretical prediction shown in Figure S2. This result is explicable with an on average shorter Sn−X bond and an upward shift of Sn s levels for FSB as exhibited in our calculations that agree satisfactorily with recent reports.[31,32]

The fluorine (1s) content appeared in the XPS survey scan when BF_4^- was incorporated into the lattice structure. We quantified the Sn:I ratio with EDX spectra in the bulk state of tin perovskites (Figure S9); the results (Table S6) showed that Sn:I ratios matched satisfactorily for both $FASnI_3$ (1:3) and FSB (1:1) species. On the surface of tin perovskites, due to the effect of Sn^{2+}/Sn^{4+} oxidation, the Sn:I ratios should be higher than the theoretical values.[7] Our XPS results (Table S6) indicated such an effect for $FASnI_3$ (1:2) and FSB (1:0.9), for which the FSB film has a ratio much closer to the theoretical one than to that of the $FASnI_3$ film. XPS for Sn species of FSB and $FASnI_3$ (Figure 2b and Figure S10) revealed the presence of Sn^{2+} and Sn^{4+} signals with disparate intensities. The proportion of Sn^{4+} in the $FASnI_3$ film surface was nearly 90%, whereas it decreased to 45% in the FSB film. The FSB perovskite has thus a greater proportion of the unoxidized Sn^{2+} state despite the same proportion of Sn^{2+} in the tin precursors (Figure S11). To confirm the stability of the materials, we recorded XRD patterns and UV−vis spectra for fresh samples and for samples exposed to ambient conditions for 4 h; the corresponding results appear in Figures S12 and S13, respectively. The UV−vis spectra of FSB show only a slight degradation for the sample aged for 4 h. In contrast, both UV−vis spectra and XRD patterns of the $FASnI_3$ film showed significant degradation upon exposure to air for 4 h.

The top view of the thin films spin-coated on an FTO substrate and their respective contact angles of the precursor solutions are shown in Figure S14. The $FASnI_{3-x}(BF_4)_x$ films showed poor film formation because of their greater contact angles except for $FASnI_3$. The solar-cell devices of a planar heterojunction type can thus not be fabricated with satisfactory performance; both $FASnI_3$ and FSB devices were fabricated according to a mesoporous carbon-electrode structure as shown in Figure 2c. The side-view SEM images of the FTO/TiO_2/Al_2O_3/C layers made of both $FASnI_3$ and FSB perovskites appear in Figure S15. The perovskites were evenly distributed with effective filling of pores in all layers. The potential energy levels of each species are shown in Figure 2d.

https://dx.doi.org/10.1021/acs.jpclett.0c00479
J. Phys. Chem. Lett. 2020, 11, 2443−2448

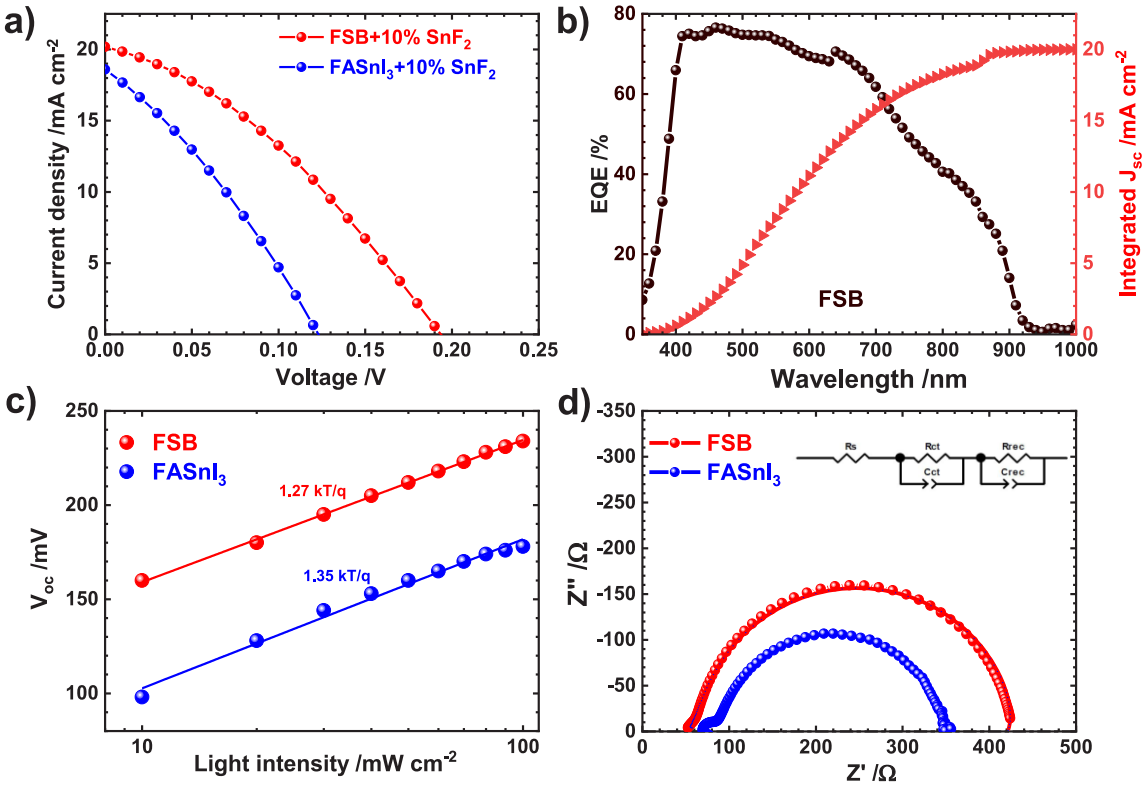

Figure 3. (a) $J-V$ curves for the best $FASnI_3$ and FSB cell. (b) IPCE with integrated current for FSB. (c) Semilogarithmic plots of the dependence of the light intensity of V_{OC} for $FASnI_3$ and FSB cells. (d) EIS spectra recorded at −0.1 V in the dark for $FASnI_3$ and FSB cells. Fitted data are shown as lines, and the corresponding equivalent circuit diagram is shown in the inset.

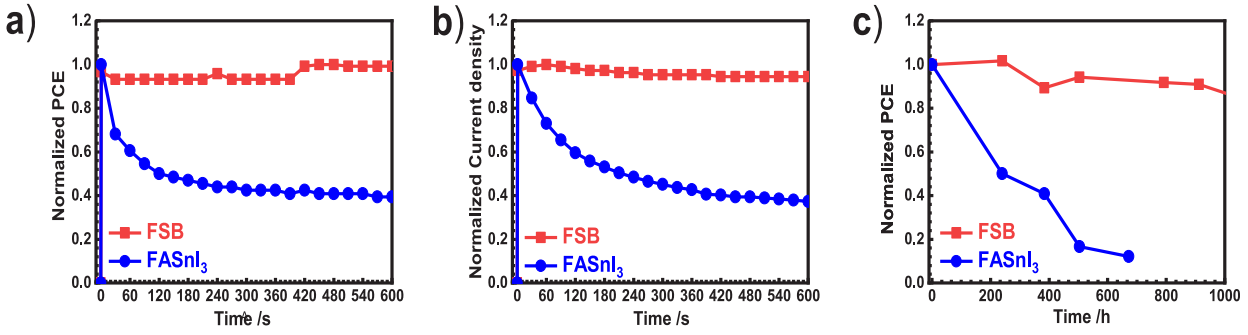

Figure 4. (a) Light-soaking effect measured under ambient conditions. (b) Maximum power-point tracking measured at 102 mV under ambient conditions. (c) Long-term dark storage stability of FSB and $FASnI_3$ devices under ambient air conditions (relative humidity of 65%).

The photovoltaic performances ($J-V$ curves) were measured for unencapsulated devices under ambient air (Figure 3a); the corresponding IPCE action spectrum for the best device of FSB is shown in Figure 3b. The obtained photovoltaic parameters, short-circuit current density (J_{SC}), open-circuit voltage (V_{OC}), fill factor (FF), and PCE, are listed in Table S7.

The results show that the V_{OC} of the FSB device improved relative to that of the $FASnI_3$ device. The J_{SC} of the FSB device also improved, consistent with the UV−vis absorption results. Both FSB and $FASnI_3$ devices showed negligible hysteresis in both forward and reverse scans (Figure S16). The integrated current from the IPCE spectrum matches satisfactorily that obtained from the $J-V$ curve. The best FSB device had a J_{SC} of 20.2 mA cm^{-2}, a V_{OC} of 194 mV, a FF of 0.34, and a PCE of 1.3%. To verify the reproducibility of our devices, Figure S17 shows box plots for 20 $FASnI_3$ and FSB devices fabricated under the same conditions. The detailed $J-V$ parameters for individual devices are listed in Tables S8 and S9. The devices made of FSB show a reproducibility greater than that for the $FASnI_3$ device. The average PCE of the FSB device (1.2 ± 0.1%) is almost twice that of the $FASnI_3$ device (0.6 ± 0.1%).

To elucidate the trends in the photovoltaic performance, we examined the slopes of plots of V_{OC} versus light intensity (Figure 3c) for both perovskite solar cells. A slope of 1.27 k_BT/q for FSB indicates the presence of Shockley−Read−Hall (SRH) recombination; the slope for devices incorporating $FASnI_3$ was greater, 1.35 k_BT/q. This effect indicates a slightly greater mitigation of the SRH recombination for the former than for the latter, primarily because of the passivation of surface traps with superhalides. We measured the dark current−voltage ($J-V$) characteristics of the two devices (Figure S18). The dark current density for FSB is one-tenth of that of the $FASnI_3$ device, indicating that more charge carriers

https://dx.doi.org/10.1021/acs.jpclett.0c00479
J. Phys. Chem. Lett. 2020, 11, 2443−2448

passed through the FSB device instead of direct shunting. The decreased leakage current and suppressed recombination of charge carriers contribute to an improved overall performance for the FSB device. The FSB device shows more diodelike behavior than the $FASnI_3$ device.[33] Nyquist plots are depicted in Figure 3d, and fitted EIS parameters of the two perovskite devices are listed in Table S10. The charge-recombination resistance (R_{rec}) was much larger for the FSB than for the $FASnI_3$ device, which contributes to the enhanced V_{OC} of the former relative to that of the latter. In summary, the substitution of I^- with BF_4^- hence significantly improved the photovoltaic performance of a superhalide perovskite device because including BF_4^- decreased the trap-assisted recombination through stronger bonding between Sn atoms and tetrafluoroborate ions, enabled efficient charge extraction, and diminished the level of surface recombination. These results agree with the recorded XPS spectra that show a suppression of Sn^{2+} oxidation.

The encapsulated device maintained almost its entire initial efficiency under one-sun irradiation for 600 s, as shown in Figure 4a. For comparison, a standard encapsulated $FASnI_3$ device lost more than half of its initial efficiency within 2 min under light-soaking conditions. Moreover, the FSB device showed stable power output for more than 600 s with a current density of >11.8 mA cm^{-2}, whereas the $FASnI_3$ device lost more than half of its initial efficiency within 2 min (Figure 4b). The FSB device maintained an almost similar performance during long-term storage even after >1000 h, whereas the efficiency of the standard $FASnI_3$ device decreased to almost nothing in 700 h (encapsulated and dark ambient air storage under 65% relative humidity) (Figure 4c). A similar trend has been reported by Tsai et al.[11] for $FASnI_3$ devices stored in a glovebox. The superior device stability might be attributed to a strong interaction as revealed by analysis of the Sn^{2+} Bader oxidation state, which gave values of 0.86 for $FASnI_3$ and 1.12 for FSB according to our calculation results.

In conclusion, we undertook the synthesis and characterization of a novel mixed halide/superhalide tin perovskite, $FASnI_{3-x}(BF_4)_x$, with a suitable band gap that yielded a device performance significantly better than that for the standard $FASnI_3$ device. The structural integrity of this perovskite is maintained as characterized by XRD, Goldschmidt tolerance factor, and plane-wave DFT calculations. The replacement of I^- with BF_4^- in the perovskite structure results in a red shift in the PL spectra through an upward shift of the VBM verified with UPS measurements. XPS data confirm the suppression of Sn^{2+}/Sn^{4+} oxidation in the FSB perovskite. The carbon-electrode PSCs fabricated with $FASnI_{3-x}(BF_4)_x$ for $x = 2$ exhibited a PCE of 1.3% (enhanced relative to 0.7% for the $FASnI_3$ device with better stability under light-soaking and dark storage conditions). The major reason for this enhancement is attributed to more rapid charge transfer and decreased recombination and background carrier density as characterized with measurements of EIS and dark $J-V$ scans. If the problem of film formation for the superhalide-based perovskite can be solved, the corresponding device performance should be greatly enhanced. Therefore, the superhalides might play an important role in producing stable tin-based PSCs with improved device performance as potential candidates for future development of lead-free perovskite solar-cell devices.

■ ASSOCIATED CONTENT

Supporting Information

The Supporting Information is available free of charge at https://pubs.acs.org/doi/10.1021/acs.jpclett.0c00479.

Experimental methods; plane-wave DFT calculations; structural analysis using XRD, SEM, XPS, UPS, and EDS; and additional device characterization methodology and procedure (PDF)

■ AUTHOR INFORMATION

Corresponding Authors

Chen Hsiung Hung − *Institute of Chemistry, Academia Sinica, Taipei 11529, Taiwan;* orcid.org/0000-0002-8060-348X; Email: chhung@gate.sinica.edu.tw

Eric Wei-Guang Diau − *Department of Applied Chemistry and Institute of Molecular Science and Center for Emergent Functional Matter Science, National Chiao Tung University, Hsinchu 30010, Taiwan;* orcid.org/0000-0001-6113-5679; Email: diau@mail.nctu.edu.tw

Authors

Mohammad Rameez − *Department of Applied Chemistry and Institute of Molecular Science, National Chiao Tung University, Hsinchu 30010, Taiwan; Institute of Chemistry and Sustainable Chemical Science and Technology (SCST), Taiwan International Graduate Program (TIGP), Academia Sinica, Taipei 11529, Taiwan*

Saeed Shahbazi − *Sustainable Chemical Science and Technology (SCST), Taiwan International Graduate Program (TIGP), Academia Sinica, Taipei 11529, Taiwan*

Putikam Raghunath − *Department of Applied Chemistry and Institute of Molecular Science, National Chiao Tung University, Hsinchu 30010, Taiwan*

Ming Chang Lin − *Department of Applied Chemistry and Institute of Molecular Science and Center for Emergent Functional Matter Science, National Chiao Tung University, Hsinchu 30010, Taiwan;* orcid.org/0000-0003-3963-6017

Complete contact information is available at: https://pubs.acs.org/10.1021/acs.jpclett.0c00479

Notes

The authors declare no competing financial interest.

■ ACKNOWLEDGMENTS

The Taiwan Ministry of Science and Technology (MOST) provided the financial support of this research (MOST 105-2119-M-009-011-MY3, MOST 107-2119-384 M-009-001, and MOST 108-2119-M-009-004). This work was also financially supported by the Center for Emergent Functional Matter Science of National Chiao Tung University from The Featured Areas Research Center Program within the framework of the Higher Education SPROUT Project of the Taiwan Ministry of Education. The National Synchrotron Radiation Research Center (NSRRC), Hsinchu Science Park, Taiwan, provided beam time for measurements of ultraviolet photoelectron spectra.

■ REFERENCES

(1) NREL. Best Research-Cell Efficiency Chart | Photovoltaic Research. https://www.nrel.gov/pv/cell-efficiency.html (accessed February 2020).

(2) Jena, A. K.; Kulkarni, A.; Miyasaka, T. Halide Perovskite Photovoltaics: Background, Status, and Future Prospects. *Chem. Rev.* **2019**, *119*, 3036−3103.
(3) Fu, H. Review of Lead-Free Halide Perovskites as Light-Absorbers for Photovoltaic Applications: From Materials to Solar Cells. *Sol. Energy Mater. Sol. Cells* **2019**, *193*, 107−132.
(4) Ke, W.; Kanatzidis, M. G. Prospects for Low-Toxicity Lead-Free Perovskite Solar Cells. *Nat. Commun.* **2019**, *10*, 965.
(5) Shi, Z.; Jayatissa, A. Perovskites-Based Solar Cells: A Review of Recent Progress, Materials and Processing Methods. *Materials* **2018**, *11*, 729.
(6) Giustino, F.; Snaith, H. J. Toward Lead-Free Perovskite Solar Cells. *ACS Energy Lett.* **2016**, *1*, 1233−1240.
(7) Kamarudin, M. A.; Hirotani, D.; Wang, Z.; Hamada, K.; Nishimura, K.; Shen, Q.; Toyoda, T.; Iikubo, S.; Minemoto, T.; Yoshino, K.; et al. Suppression of Charge Carrier Recombination in Lead-Free Tin Halide Perovskite via Lewis Base Post-Treatment. *J. Phys. Chem. Lett.* **2019**, *10*, 5277−5283.
(8) Diau, E. W.-G.; Jokar, E.; Rameez, M. Strategies To Improve Performance and Stability for Tin-Based Perovskite Solar Cells. *ACS Energy Lett.* **2019**, *4*, 1930−1937.
(9) Tsai, C.-M.; Mohanta, N.; Wang, C.-Y.; Lin, Y.-P.; Yang, Y.-W.; Wang, C.-L.; Hung, C.-H.; Diau, E. W.-G. Formation of Stable Tin Perovskites Co-Crystallized with Three Halides for Carbon-Based Mesoscopic Lead-Free Perovskite Solar Cells. *Angew. Chem., Int. Ed.* **2017**, *56*, 13819−13823.
(10) Jokar, E.; Chien, C.-H.; Tsai, C.-M.; Fathi, A.; Diau, E. W.-G. Robust Tin-Based Perovskite Solar Cells with Hybrid Organic Cations to Attain Efficiency Approaching 10%. *Adv. Mater.* **2019**, *31*, 1804835.
(11) Tsai, C.-M.; Lin, Y.-P.; Pola, M. K.; Narra, S.; Jokar, E.; Yang, Y.-W.; Diau, E. W.-G. Control of Crystal Structures and Optical Properties with Hybrid Formamidinium and 2-Hydroxyethylammonium Cations for Mesoscopic Carbon-Electrode Tin-Based Perovskite Solar Cells. *ACS Energy Lett.* **2018**, *3*, 2077−2085.
(12) Jokar, E.; Chien, C.-H.; Fathi, A.; Rameez, M.; Chang, Y.-H.; Diau, E. W.-G. Slow Surface Passivation and Crystal Relaxation with Additives to Improve Device Performance and Durability for Tin-Based Perovskite Solar Cells. *Energy Environ. Sci.* **2018**, *11*, 2353−2362.
(13) Ke, W.; Stoumpos, C. C.; Zhu, M.; Mao, L.; Spanopoulos, I.; Liu, J.; Kontsevoi, O. Y.; Chen, M.; Sarma, D.; Zhang, Y.; et al. Enhanced Photovoltaic Performance and Stability with a New Type of Hollow 3D Perovskite {en}FASnI$_3$. *Sci. Adv.* **2017**, *3*, No. e1701293.
(14) Sabba, D.; Mulmudi, H. K.; Prabhakar, R. R.; Krishnamoorthy, T.; Baikie, T.; Boix, P. P.; Mhaisalkar, S.; Mathews, N. Impact of Anionic Br $^-$ Substitution on Open Circuit Voltage in Lead Free Perovskite ($CsSnI_{3-x}Br_x$) Solar Cells. *J. Phys. Chem. C* **2015**, *119*, 1763−1767.
(15) Hendon, C. H.; Yang, R. X.; Burton, L. A.; Walsh, A. Assessment of Polyanion (BF_4^- and PF_6^-) Substitutions in Hybrid Halide Perovskites. *J. Mater. Chem. A* **2015**, *3*, 9067−9070.
(16) Chen, J.; Kim, S.-G.; Park, N.-G. $FA_{0.88}Cs_{0.12}PbI_{3-x}(PF_6)_x$ Interlayer Formed by Ion Exchange Reaction between Perovskite and Hole Transporting Layer for Improving Photovoltaic Performance and Stability. *Adv. Mater.* **2018**, *30*, 1801948.
(17) Nagane, S.; Ogale, S. $CH_3NH_3Pb(BF_4)_3$ and $(C_4H_9NH_3)_2Pb(BF_4)_4$ Family of 3D and 2D Perovskites without and with Iodide and Bromide Ions Substitution. *J. Phys. Chem. Lett.* **2016**, *7*, 4757−4762.
(18) Zhang, J.; Wu, S.; Liu, T.; Zhu, Z.; Jen, A. K.-Y. Boosting Photovoltaic Performance for Lead Halide Perovskites Solar Cells with BF_4^- Anion Substitutions. *Adv. Funct. Mater.* **2019**, *29*, 1808833.
(19) Nagane, S.; Bansode, U.; Game, O.; Chhatre, S.; Ogale, S. $CH_3NH_3PbI_{(3-x)}(BF_4)_x$: Molecular Ion Substituted Hybrid Perovskite. *Chem. Commun.* **2014**, *50*, 9741.
(20) Chen, J.; Rong, Y.; Mei, A.; Xiong, Y.; Liu, T.; Sheng, Y.; Jiang, P.; Hong, L.; Guan, Y.; Zhu, X.; et al. Hole-Conductor-Free Fully Printable Mesoscopic Solar Cell with Mixed-Anion Perovskite $CH_3NH_3PbI_{(3-x)}$ $(BF_4)_x$. *Adv. Energy Mater.* **2016**, *6*, 1502009.
(21) Sheng, Y.; Mei, A.; Liu, S.; Duan, M.; Jiang, P.; Tian, C.; Xiong, Y.; Rong, Y.; Han, H.; Hu, Y. Mixed $(5\text{-AVA})_xMA_{1-x}PbI_{3-y}(BF_4)_y$ Perovskites Enhance the Photovoltaic Performance of Hole-Conductor-Free Printable Mesoscopic Solar Cells. *J. Mater. Chem. A* **2018**, *6*, 2360−2364.
(22) Xiang, J.; Wang, K.; Xiang, B.; Cui, X. Sn^{2+}- Stabilization in $MASnI_3$ Perovskites by Superhalide Incorporation. *J. Chem. Phys.* **2018**, *148*, 124111.
(23) Stoumpos, C. C.; Malliakas, C. D.; Kanatzidis, M. G. Semiconducting Tin and Lead Iodide Perovskites with Organic Cations: Phase Transitions, High Mobilities, and Near-Infrared Photoluminescent Properties. *Inorg. Chem.* **2013**, *52*, 9019−9038.
(24) Travis, W.; Glover, E. N. K.; Bronstein, H.; Scanlon, D. O.; Palgrave, R. G. On the Application of the Tolerance Factor to Inorganic and Hybrid Halide Perovskites: A Revised System. *Chem. Sci.* **2016**, *7*, 4548−4556.
(25) Fang, Z.; Yi, Z. First Principles Study on Mixed Orthorhombic Perovskite $CH_3NH_3Pb(I_{1-X}Br_x)_3$. *Chem. Phys. Lett.* **2017**, *687*, 19−22.
(26) Shi, T.; Zhang, H.-S.; Meng, W.; Teng, Q.; Liu, M.; Yang, X.; Yan, Y.; Yip, H.-L.; Zhao, Y.-J. Effects of Organic Cations on the Defect Physics of Tin Halide Perovskites. *J. Mater. Chem. A* **2017**, *5*, 15124−15129.
(27) Liao, Y.; Liu, H.; Zhou, W.; Yang, D.; Shang, Y.; Shi, Z.; Li, B.; Jiang, X.; Zhang, L.; Quan, L. N.; et al. Highly Oriented Low-Dimensional Tin Halide Perovskites with Enhanced Stability and Photovoltaic Performance. *J. Am. Chem. Soc.* **2017**, *139*, 6693−6699.
(28) Burt, J.; Grantham, W.; Levason, W.; Light, M. E.; Reid, G. Hexafluorosilicate and Tetrafluoroborate Coordination to Lead (II) Di- and Tri-Imine Complexes − Unusual Fluoroanion Coordination Modes. *Polyhedron* **2015**, *85*, 530−536.
(29) Krossing, I.; Raabe, I. Noncoordinating Anions—Fact or Fiction? A Survey of Likely Candidates. *Angew. Chem., Int. Ed.* **2004**, *43*, 2066−2090.
(30) Kato, M.; Fujiseki, T.; Miyadera, T.; Sugita, T.; Fujimoto, S.; Tamakoshi, M.; Chikamatsu, M.; Fujiwara, H. Universal Rules for Visible-Light Absorption in Hybrid Perovskite Materials. *J. Appl. Phys.* **2017**, *121*, 115501.
(31) Tao, S.; Schmidt, I.; Brocks, G.; Jiang, J.; Tranca, I.; Meerholz, K.; Olthof, S. Absolute Energy Level Positions in Tin- and Lead-Based Halide Perovskites. *Nat. Commun.* **2019**, *10*, 2560.
(32) Ke, W.; Stoumpos, C. C.; Logsdon, J. L.; Wasielewski, M. R.; Yan, Y.; Fang, G.; Kanatzidis, M. G. TiO_2−ZnS Cascade Electron Transport Layer for Efficient Formamidinium Tin Iodide Perovskite Solar Cells. *J. Am. Chem. Soc.* **2016**, *138*, 14998−15003.
(33) Li, C.; Song, Z.; Zhao, D.; Xiao, C.; Subedi, B.; Shrestha, N.; Junda, M. M.; Wang, C.; Jiang, C.-S.; Al-Jassim, M.; et al. Reducing Saturation-Current Density to Realize High-Efficiency Low-Bandgap Mixed Tin-Lead Halide Perovskite Solar Cells. *Adv. Energy Mater.* **2019**, *9*, 1803135.

https://dx.doi.org/10.1021/acs.jpclett.0c00479
J. Phys. Chem. Lett. 2020, 11, 2443−2448